R. Albarracin, G. Robles, J.M. Martinez-Tarifa, J. Ardila-Rey (2015). Separation of sources in radiofrequency measurements of partial discharges using time-power ratios maps, in *ISA Transactions* [Available online 18 May 2015].
http://dx.doi.org/10.1016/j.isatra.2015.04.006

Separation of sources in radiofrequency measurements of partial discharges using time–power ratio maps

R. Albarracin [a,*], G. Robles [a,**], J.M. Martinez-Tarifa [a], J. Ardila-Rey [b]

[a] Department of Electrical Engineering, Universidad Carlos III de Madrid, Leganés -28911, Spain

[b] Department of Electrical Engineering, Universidad Técnica Federico Santa María, Santiago de Chile, Chile

Abstract: Partial discharges measurement is one of the most useful tools for condition monitoring of high-voltage (HV) equipment. These phenomena can be measured on-line in radiofrequency (RF) with sensors such as the Vivaldi antenna, used in this paper, which improves the signal-to-noise ratio by rejecting FM and low-frequency TV bands. Additionally, the power ratios (PR), a signal-processing technique based on the power distribution of the incoming signals in frequency bands, are used to characterize different sources of PD and electromagnetic noise (EMN). The calculation of the time length of the pulses is introduced to separate signals where the PR alone do not give a conclusive solution. Thus, if several EM sources could be previously calibrated, it is possible to detect pulses corresponding to PD activity.

Keywords: Partial discharges, Dielectric materials, Condition monitoring, RF measurements, VHF and UHF measurements, Vivaldi antennas, Spectral power.

1. Introduction

The insulation systems of electrical assets are subjected to mechanical, thermal and electrical stresses that degrade their behaviour and can lead to unexpected equipment outages and failures, such as in rotating machines [1]. Knowing the condition of the insulation is key for the reliability of power systems [2]. Partial discharges (PD) are low-energy ionizations in sites where highly divergent fields are present [3], so they represent a measurable manifestation of electrical stress and a symptom of other problems in the electrical asset. They are classified into three groups: corona, surface and internal [4]. Corona PD often occur in sharp metallic structures under high-voltage stress. Surface PD may also occur in inhomogeneous locations on dielectrics when there exist a tangential component of the electric field parallel to the dielectric surface. And, finally, the most harmful PD for electrical insulation are internal, occurring in gas filled cavities inside the dielectric, due to imperfections in the manufacturing process, installation or external damages. In addition, its continued activity gradually degrades the insulation system in which they occur leading to a total discharge and the breakdown of the electrical equipment. Therefore, the detection of PD activity is an important test for determining the quality of the insulation system [5]. Moreover, the analysis of partial discharges helps us to perform a correct condition-based maintenance (CBM) of power system assets such as air-insulated substations (AIS) and gas-insulated substations (GIS), transformers, power cables, motors and generators.

One immediate consequence of the PD activity is an electromagnetic (EM) emission in the very-high-frequency (VHF) and ultra-high-frequency (UHF) bands, 30–300 MHz and 300–3000 MHz, respectively, that can be measurable in RF with disc couplers and antennas [6,7]. The use of EM sensors can be applied to any type of insulating material with the advantage of not needing a galvanic connection to the equipment when compared with capacitive and inductive sensors. Moreover, the nature of an insulating dielectric can be related to the frequency band emitted by the PD, being their energy higher at high frequencies for stronger dielectrics than for weaker insulations [8].

On the other hand, the advantage of galvanic insulation turns into a disadvantage when the phase of the sinusoidal voltage is needed to find out what type of PD is active. This is usually done with phase resolved partial discharge (PRPD) patterns where the amplitude of the pulse versus the phase referred to the applied voltage are plotted, and the type of PD is identified through the pattern it draws [4]. Additionally, there is not a clear relationship between the power emitted by the PD and the power received by

* Corresponding author. Tel.: +34 653204691.

** Corresponding author. Tel.: +34 916245922; fax: +34 916249430.

E-mail addresses: rasbarracin@gmail.com (R. Albarracin), grobles@ing.uc3m.es (G. Robles), jmmtarif@ing.uc3m.es (J.M. Martinez-Tarifa), jorge.ardila@usm.cl (J. Ardila-Rey).

the antenna. This loss of information makes it difficult to separate the signals of interest from other interferences (considered, henceforth, as noise). The electromagnetic noise (EMN) can be classified into several categories:

- Continuous sinusoidal noise from communication systems such as FM radio, digital TV, Digital Audio Broadcasting (DAB), Global System for Mobile communications (GSM) and Wi-Fi, which can hide the sources of PD and even can be superimposed to PD pulses. All sources together emit energy in a broadband so their filtering can be laborious as well as the subsequent separation from PD.
- Stochastic noise, random both in time and amplitude such as corona in air, that can emit energy up to 500 MHz, though in most cases they only reach 250 MHz [9] sparking and lamp ignition.
- Periodic-pulsing noise from thyristor operation, i.e. inverters in electrical motors and voltage or current regulated sources.

For these reasons, the characterization of PD in RF is an open and current research topic whose challenge is the possibility of separating different EM sources. All current methods are based on the frequency characteristics of the emitted signals and what changes is the way they represent the differences. In some cases, these representations are based on triangles in which every side is a frequency band at low, medium and high frequencies. In [10], the curves represented in these ternary plots are not absolute values for the magnitude of every source but relative values to each of the sources. In [11], the representation is again in a ternary plot, this time with the energy of the signals. In [12], the representation is based on a time–frequency map already used in measurements with high-frequency transformers in conventional methods with PRPD. Finally, in [13], support vector machines are used to classify signals but a previous training of the SVM is needed.

The proposed algorithm represents the differences in frequency in only two dimensions so one of its main characteristics is its simplicity and the facility to extract conclusions from the representation map. Moreover, when the spectra are very similar and cannot separate the sources, it is complemented with the time duration of the signals. In this sense, the aim is that the separation technique integrates calculations with low computational load to open the possibility to be implemented in Field-Programmable Gate Arrays (FPGA) or in low-cost microprocessors.

In this paper, the use of a specific sensor together with an ad-hoc signal-processing technique is proposed to separate several PD sources and electromagnetic noise (EMN). First, Vivaldi antennas, due to their constructive nature, allow us to mitigate FM radio and low-frequency TV broadcasting bands. Second, the spectral Power Ratios (PR) [14] were selected as a low computational load tool to isolate the measured sources. With this aim, measurements of corona and surface PD have been carried out when two EM sources of disturbances are present. Their power spectral content in two bands of frequency (low-frequency and high-frequency) is plotted in a two-dimension map to separate the signals. It may occur that some EM sources have power in the same frequency bands so they cannot be easily separated. The observation of the signals shows that certain powerful interferences such as sparking due to relays and lamps ignition always have long duration pulses while their frequency content remains in the same band as PD. Hence, this paper proposes the use of the time duration of the pulses as a third variable when two dimensions are not successful in the separation of the sources. Moreover, if several EM sources are previously characterized, it is possible to identify pulses from other sources that very likely could come from PD activity.

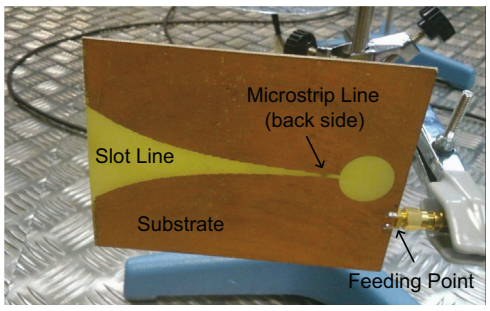

Fig. 1. Vivaldi antenna layout.

2. Vivaldi antenna

Vivaldi antennas are aperture-planar antennas that use two pieces of copper, each one aside of a dielectric substrate [15]. This sensor is a waveguide, or slot line, of small size integrated into a dielectric substrate and an appropriate transition from a feeding transmission line installed in the antenna as depicted in Fig. 1. These antennas are not resonant in nature and broad bandwidth can be achieved with low return losses by optimizing the profile of the slot and the feeding network. Moreover, this antenna has a directive pattern with linear polarization that allows us to be more selective in pulse acquisitions if the sensor is set pointing to the EM emitter.

In this case, a Vivaldi antenna with a total size of 9 cm $\times$ 12 cm was originally designed and optimized to operate centred around 2 GHz. The dimensions of this sensor are chosen according to the restrictions summarized in [16] and to operate in compliance with the requirements of the measurement of PD in UHF. The antenna was manufactured by photolithography in a FR4 dielectric substrate with a thickness of 1.5 mm. Not only is this sensor an inexpensive alternative to log-periodic antennas, but also its behaviour is better than log-periodic and monopole antennas [17]. The reason is that this Vivaldi antenna, adapted for high frequencies, can also measure EM pulses with low-frequency content where corona and surface PD emit power. Thus, these types of antennas mitigate the background interference of FM radio and the low frequencies band of TV broadcasting and, furthermore, they are able to measure PD in a broader band of frequencies than monopole antennas because of their non-resonant nature.

The emitter–channel–receiver system in which the antenna works can be represented by a quadrupole by using the scattering parameters [18]. In this equivalent circuit, the return losses of the antenna are obtained from the measurement of the reflection parameter, S_{11}. When S_{11} =0 dB all the power is reflected and for values more negatives than −10 dB the sensor is considered to be matched. To measure the return losses for the manufactured prototype, an Agilent Technologies E8364B Network Analyser is used and its reflection parameter is shown in Fig. 2. As it can be seen, the antenna is matched in the range between 1.3 GHz and 3 GHz. Besides, the antenna has S_{11} values close to −10 dB in the 0.7–1.2 GHz range and between −5 dB and −8 dB in the 0.6–0.7 GHz range which permits us to acquire pulses with power at those frequencies, however mitigated. For frequencies lower than 0.4 GHz, the reflection parameter is greater than −2 dB, so the Vivaldi antenna works as a high-pass filter. Thus, frequency components from FM radio (the EM noise source with higher amplitude) are attenuated in more than 15 dB compared to other high-frequency components.

3. Experimental setup

Partial discharges were created with two test objects specifically designed to generate surface and corona pulses when high-voltage is applied. The HV source is a Schleich BV 702210 transformer with a GLP1-e HV control module that can reach up to 18 kV, greater than the partial discharge inception voltage (PDIV) of the test objects. Every test object was previously tested in a setup according to the indirect circuit in Standard IEC-60270 and PD were acquired with a commercial PD analyser to register and verify the PD activity. During the measurements, two RF external perturbations were activated to study their influence in simultaneous acquisitions from the two PD sources. A laptop Wi-Fi receptor was switched on and a set of six lamps with three fluorescent lamps of 18 W each one was turned on and off during the measurements. The antenna was placed at a distance of 1 m from the test objects and connected to a Tektronix DPO 7254 oscilloscope with a sampling frequency of 40 GS/s and a bandwidth of 2.5 GHz. Each of the elements described above is shown in Fig. 3.

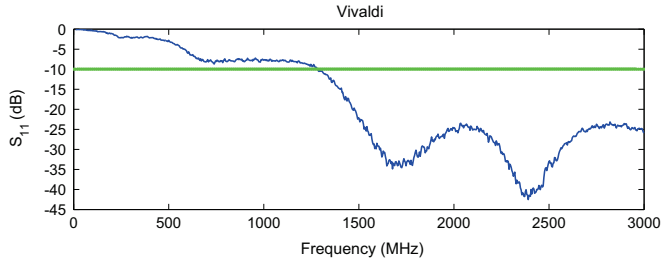

Fig. 2. Reflection parameter S_{11} of the Vivaldi antenna.

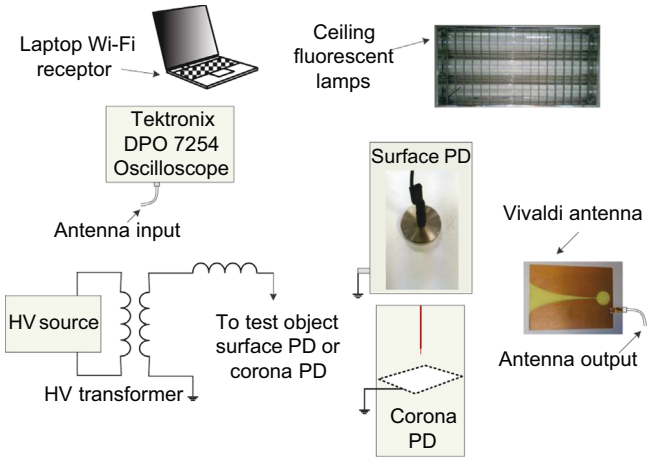

Fig. 3. Experimental setup for measuring corona, surface PD and two kinds of EMN sources using a Vivaldi antenna.

4. Test objects design

The first test object is an electrode connected to the HV source placed on a layer of polyethylene. This configuration simulates the type of defect that can occur on the interface of two dielectrics, usually between solid dielectric and air. It is very common to find these surface PD on contaminated surfaces of dielectrics and between windings of electrical machines such as motors and other

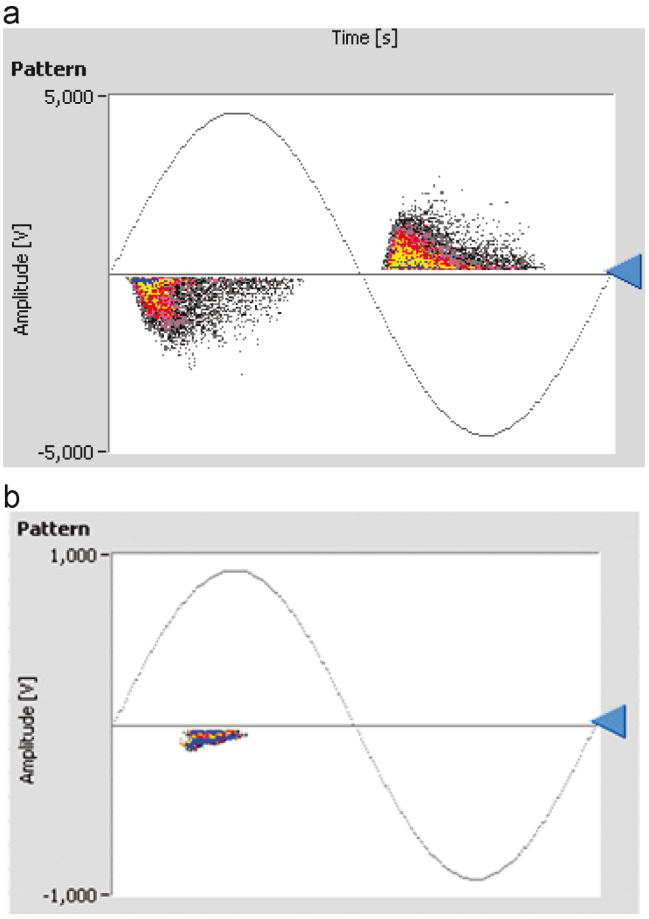

Fig. 4. PRPD pattern of (a) Surface PD on polyethylene sheet and (b) Corona PD in point-plane configuration.

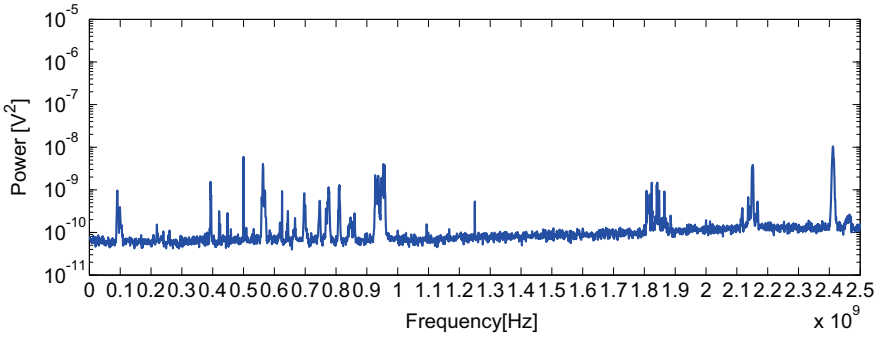

Fig. 5. Background EMN measured by Vivaldi antenna.

metals under electric stress. In this case, the PDIV was found to be above 1.4 kV, so the applied voltage was 1.5 kV.

The second test object consists of a copper wire 0.2 cm in diameter sharp-ended and separated 2 cm from ground. This test object represents corona PD that may appear on sharp elements when HV is applied in electrical equipment. The PDIV was found to be above 12 kV for positive corona and the applied voltage was 13 kV where there were a high activity of corona PD that could be measured by the antenna.

In both cases, the activity and the type of discharge were checked with the commercial PD acquisition system confirming surface PD in the first case and corona PD for the second, as can be seen in their phase-resolved partial discharge patterns in Fig. 4 [19].

5. Signal processing

The aim of the algorithm is to extract frequency characteristics that can help us to distinguish between signals by using the PR maps and to complement this technique with the time duration of the pulse when the frequency characteristics are not sufficient to separate events.

The previous step is to normalize the signal with time, $s(t)$, using

$$\tilde{s}(t) = \frac{s(t)}{\sqrt{\int_0^T s(t)^2\, dt}} \tag{1}$$

with T being the time window in which the event is registered and $\tilde{s}(t)$ is the normalized signal.

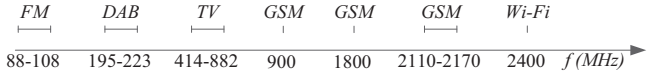

Fig. 6. Frequency bands of the background EMN.

5.1. Spectral power analysis

The PR technique uses two bands of frequency where there are significant differences between signals [14]. In this case, the accumulated spectral power is

$$\%PRL = \sum_{f=f_{1_L}}^{f_{2_L}} |\tilde{S}(f)|^2 \times 100 \tag{2}$$

$$\%PRH = \sum_{f=f_{1_H}}^{f_{2_H}} |\tilde{S}(f)|^2 \times 100 \tag{3}$$

considering that the total power of the signal is 1 because it has been normalized. PRL and PRH are the power ratios for the low-frequency, $[f_{1_L}, f_{2_L}]$, and high-frequency, $[f_{1_H}, f_{2_H}]$, bands, respectively. The two bands can be set according to the frequency characteristics of the signal. $|\tilde{S}(f)|$ is the fast Fourier transform (FFT) value of the PD normalized pulse.

The PRL and PRH parameters are plotted in a 2D map to separate EM sources different from noise and EMN. Once the separation is satisfactory, the signals in a cluster are selected and represented in a PRPD pattern [14]. Unfortunately, in most cases, when PD measurements are done in RF, it is not possible to have access to a grid voltage reference to obtain the PRPD. To overcome this drawback, the approach in this paper is based on the previous characterization of all EM sources through a PR map when all PD sources are inactive. Then, other EM sources that may appear later placing the antenna close to a potential PD source will very likely come from the activity of PD and will have their position in the map.

5.2. Signal time duration

In some cases, two or more EM sources can be overlapped and it may be necessary to obtain additional information from the time characteristics of the measured pulse such as its total time duration.

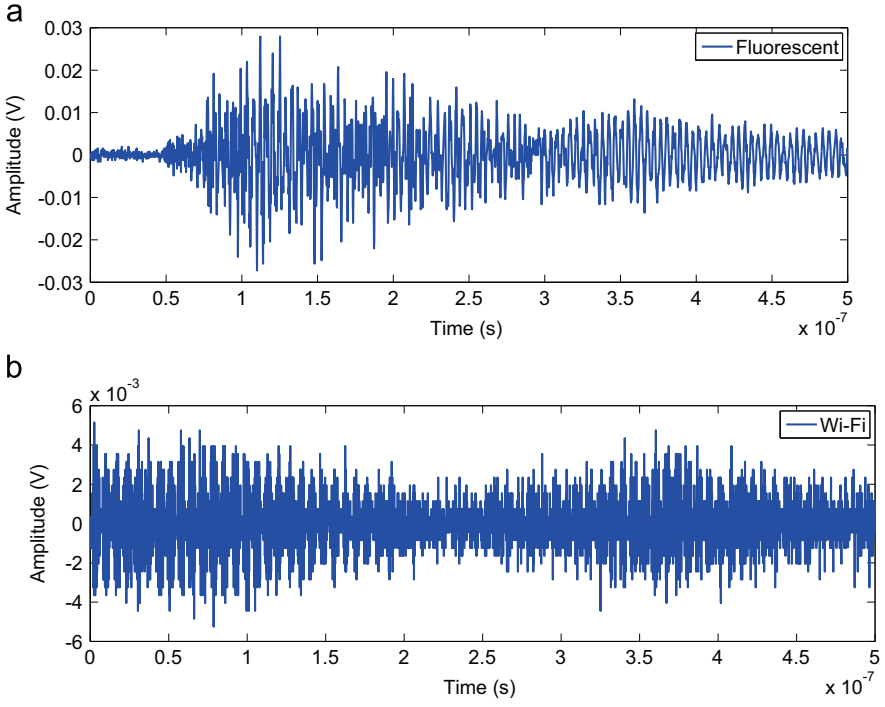

Fig. 7. RF pulses measured by the Vivaldi antenna: (a) fluorescent lamp ignition and (b) Wi-Fi.

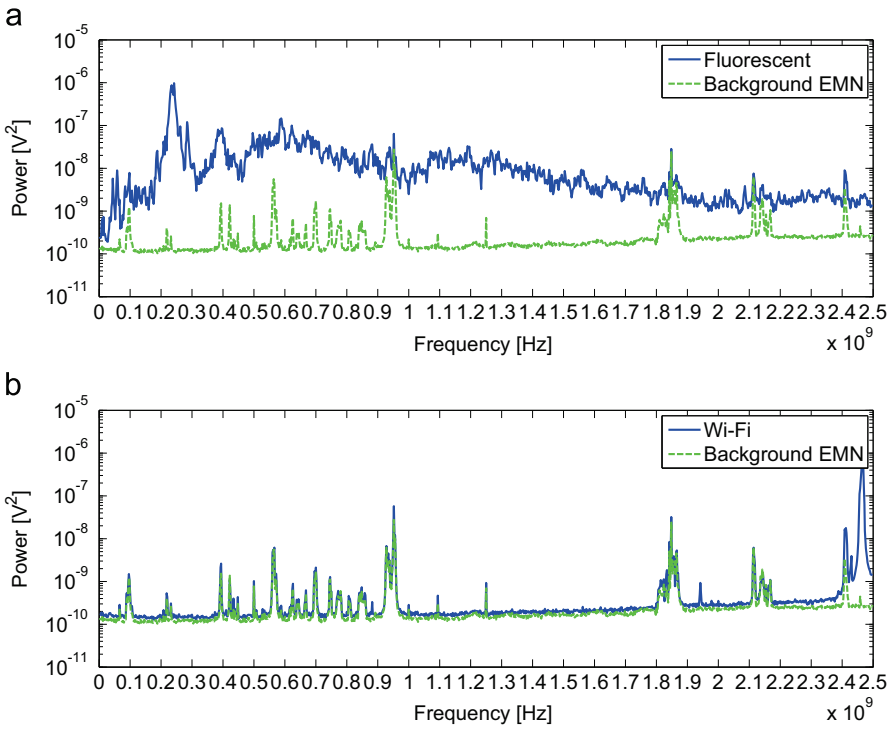

Fig. 8. Power spectrum of RF pulses measured by the Vivaldi antenna: (a) fluorescent lamp ignition and (b) Wi-Fi compared to the EMN floor.

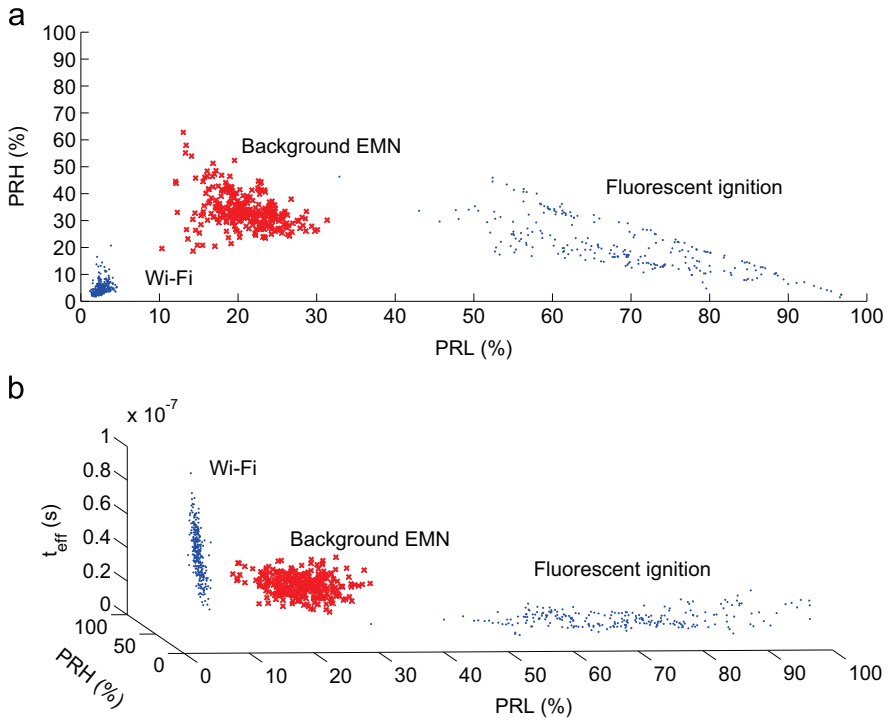

Fig. 9. (a) PR and (b) PR–time maps for the background EMN, Wi-Fi and fluorescent lamps emissions measured by the Vivaldi antenna.

Once calculated, it may be included in the PRL–PRH map to add a third dimension to enable a better separation between clusters.

The effective pulse width (t_{eff}) is used to calculate the equivalent time length from each pulse. This time corresponds to the width of a rectangular pulse with the same peak as the squared signal and whose integral gives the same energy, so both have the same area. The time t_{eff} is calculated as follows:

$$t_{eff} = \frac{\int_0^T \tilde{s}(t)^2\, dt}{\tilde{s}(t)^2_{max}} = \frac{1}{\tilde{s}(t)^2_{max}} \tag{4}$$

where the numerator of the fraction is the integral value of the

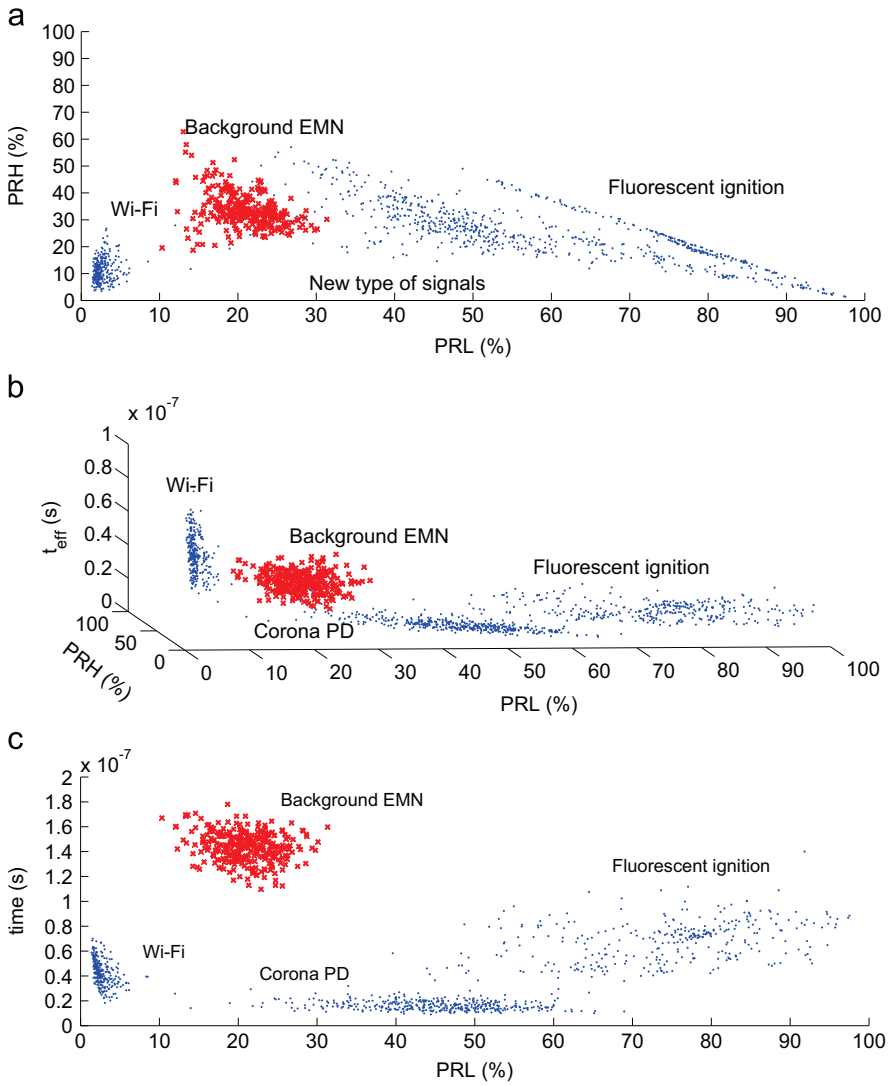

Fig. 10. (a) Power ratio map, (b) PR–time map and (c) PRL–time map for fluorescent lamp ignition pulses, Wi-Fi, corona PD source and EMN.

pulse for the entire acquisition window, being 1 because it is normalized and $\tilde{s}(t)_{max}$ is the maximum value of the signal.

6. Measurements and results

Partial discharges from each test object, Wi-Fi interferences and lighting of fluorescent lamps were acquired simultaneously with the Vivaldi antenna. The EMN is also included from other acquisitions campaign. The measuring method is performed so as to obtain reliable and comparable acquisitions. The oscilloscope registered and saved 1000 signals in the time domain with a sampling frequency of 5 GS/s and a time window of $T = 0.5$ μs.

6.1. Background noise and disturbances characterization

Before the acquisition of PD, the background EMN has to be characterized and identified. Its averaged spectrum, represented in Fig. 5, is obtained from their normalized pulses and the frequency bands of interest are defined in Fig. 6 up to 2.5 GHz. As it can be seen from its spectrum, Fig. 5, these pulses have a poor response at low frequencies as expected, so the FM radio effect is notably reduced. This is a clear advantage both in time and frequency when acquiring PD in RF with the Vivaldi antenna.

Other EM sources of disturbance can difficult the measurement of PD such as sparking and relay commutations. Pulses from the lighting of fluorescent lamps are acquired when the switch is turned on. When the electronic ballast that feeds the lamp is started, produces fast arcs and sparks that are measurable in RF. Note that, fluorescent lamps during its normal operation and when they are switched off do not emit measurable pulses in RF. An energy normalized pulse and its spectrum are presented in Fig. 7(a) and 8(a), respectively.

The second EM source of disturbance studied is a Wi-Fi receiver in a laptop that is activated when the measurement campaign is started and is close enough to the antenna in the laboratory so their pulses have sufficient amplitude to trigger the oscilloscope acquisition. This kind of EMN source can be present in field measurements when a laptop is necessary for the RF acquisition system. Its energy normalized pulse and its spectrum are shown in Figs. 7(b) and 8(b), respectively.

Due to the fact that both disturbances, Wi-Fi (when the receiver is activated) and fluorescent lamp emissions, can be controlled they can be studied separately and simultaneously to corroborate where their clusters are located in the 2D and 3D PR maps.

Since the frequency ranges in which the separation on the PR map is satisfactory are not known, it is necessary to calculate the FFT of all pulses and compare the most representative spectra with

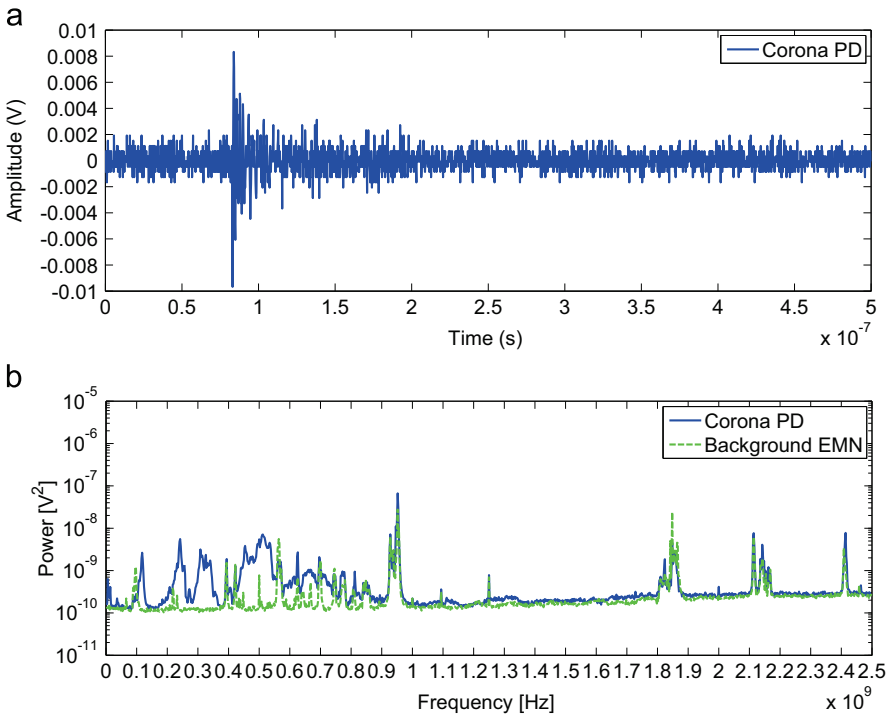

Fig. 11. RF pulse from the first PD source and its spectrum. (a) Corona PD pulse and (b) Corona PD spectrum.

the EMN floor and to each other. This will determine which frequency bands have significant changes. For all cases studied, a good separation is achieved with the following frequency values: f_{1L}=120 MHz, $f_{2L}=f_{1H}=850$ MHz and $f_{2H}=1700$ MHz.

All disturbances are plotted together in a PR map and in a PR–time map, Fig. 9(a) and (b), respectively. As it can be seen, it is possible to identify three different clusters: background EMN, Wi-Fi receiver and fluorescent lamp emissions.

The background EMN is the easiest to locate because it is always present and a simple measurement in an open area without other emission will be enough to characterize its position. For the low and high frequency intervals given above, the EMN cluster has the following parameters: PRL=10–31%, PRH=18.7–62.8% and t_{eff}=18–49 ns, with an average value of 32.6 ns. Notice, that being interferences from radio and TV broadcasting, the equivalent time durations will be long.

Wi-Fi is a 2.4 GHz modulated signal so its power is almost not taken into account for the chosen intervals. Then, it is shown as a cluster located at low PRL and PRH values, from 1.5 to 6% while the equivalent time duration is the longest, with an average value of 58 ns.

The fluorescent lamps ignition pulses, and in general, sparking and relay commutation, are characterized by short to medium duration pulses and high dispersion of power in all the band of frequencies. In this case t_{eff}=3.6–33 ns, and 14.8 ns of average value, with high PRL values in the range of 40–98%.

6.2. Measurements with the antenna and separation of multiple EM sources

Once the background EMN and the disturbances have been characterized, partial discharges are measured simultaneously with disturbances by applying HV to the corona and the surface PD test objects individually. During the acquisitions, the fluorescent lamps are successively switched on and off and the Wi-Fi receptor is activated.

6.3. Pulse separation

6.3.1. Corona PD, Wi-Fi and fluorescent lamps ignition

In this experiment all disturbing sources are active with the point-plane test object energized at 13 kV. The position of all disturbances does not change so it is clear that the new cluster that appears in the plot in Fig. 10(a) comes from the new corona EM source.

This corona cluster intersects slightly with the fluorescent lamp and EMN clusters and the border is not clear in some areas. Even under these circumstances, the PR map representation would be enough to separate all sources. If the pulse duration is added as a third dimension, Fig. 10(b), the clusters appear clearly separated and it is possible to distinguish the multiple sources. Moreover, the PRL–time view of the 3D map, Fig. 10(c), gives a better perspective of all events in which the clusters are even more separated.

Corona PD are characterized by short time durations with t_{eff}=2.8–18 ns, while its average value is 7.3 ns, so they are clearly distinguishable from other clusters. The power is also dispersed through all the spectra from 100 to 900 MHz, approximately so the pulses are represented in a cluster in the ranges of PRL=22–70%, PRH=14.6–57%. One example of a corona pulse in the time and frequency domains is represented in Fig. 11(a) and (b), respectively.

6.3.2. Surface PD, Wi-Fi and fluorescent lamp ignition

This experiment includes the effect of the surface partial discharges in the polyethylene test object. Notice that the PRL-PRH map in Fig. 12(a) shows that the interferences (Wi-Fi receptor, the fluorescent lamp ignition and the background EMN emissions) are located in the same zones as before because the frequency intervals, PRL (120–850 MHz) and PRH (850–1700 MHz), have not been changed. Unfortunately, the cluster of surface discharges is located in an area that it is already occupied by two other sources, especially the background EMN, so the final cloud of points is

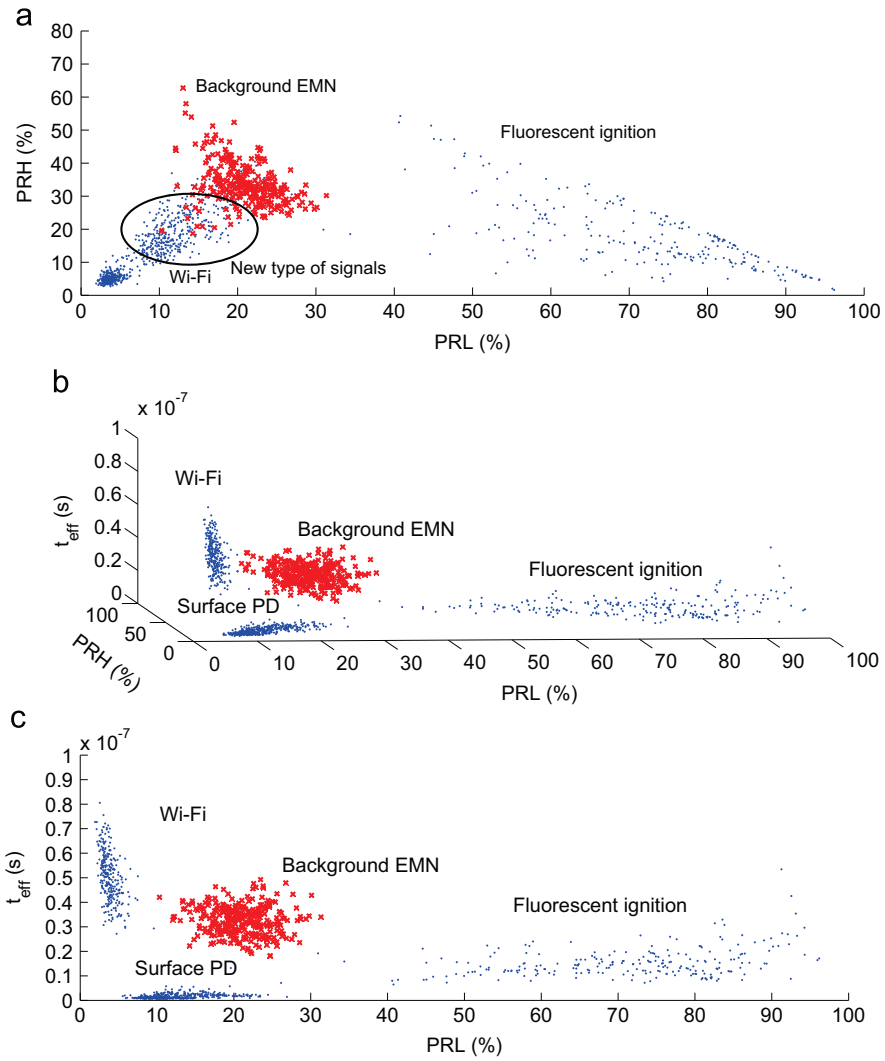

Fig. 12. (a) Power ratio map, (b) PR–time map and (c) PRL–time map for fluorescent lamp ignition pulses, Wi-Fi, surface PD source and EMN.

impossible to separate. Including the time duration t_{eff}, Fig. 12 (b) and 12(c), the clusters appear separated and surface PD with very short time durations t_{eff}=0.7–5.7 ns, being 2 ns its average value, are located at the bottom of the 3D map. These effective times are the shortest of all measured events, so even having power in coincident bands with other sources (PRL=6–25% and PRH=9–41%) surface discharges can been separated.

Fig. 13(a) shows a surface PD pulse where its short duration can be appreciated. Finally, Fig. 13(b) shows that it has power in all the frequency bands.

To summarize, all results are included in Table 1, where the values of PRL, PRH and average time duration for each EM source are included.

7. Conclusions

The main drawback of the EM PD condition monitoring is that, in most cases, it is not possible to obtain a PRPD because there is not voltage grid synchronization. In this paper, it has been found that all sources have characteristics that permit their recognition and differentiation from each other. The Wi-Fi has the larger time duration followed by the EMN and the fluorescent lamp ignition emissions. The fluorescent lamp pulse has the highest amplitude, reaching 30 mV, whereas the EMN has the lowest, lower than Wi-Fi pulses at 6 mV. Generally, PD pulses are characterized by extremely short rise times that are translated into electromagnetic pulses with very short time lengths. Corona and surface PD signals have mid-range amplitudes and the shortest durations. Only in the case of having important multipath propagations, these pulses would be longer in time and the antenna should be moved around for an optimum characterization. Considering all these characteristics, the separation is more effective if the differences in time are taken in account.

The power distribution in frequency for the pulses from the fluorescent lamp is located in a wide band mainly from 300 MHz to 2500 MHz. On the other side, the Wi-Fi pulses have power mainly for 2.4 GHz. Corona PD emit power in the 100–900 MHz band though most of it is in the 200–600 MHz range. Surface PD power in the polyethylene test object ranges from 200 MHz to 2500 MHz.

From these results, it is clear that it is possible to separate clusters and if the EM disturbances are known and catalogued, PD can also be identified. Besides, PD from two controlled PD test objects can also be separated and further processed to identify their nature.

In summary, if several of the EM disturbance sources are isolated and previously characterized, it is possible to detect pulses

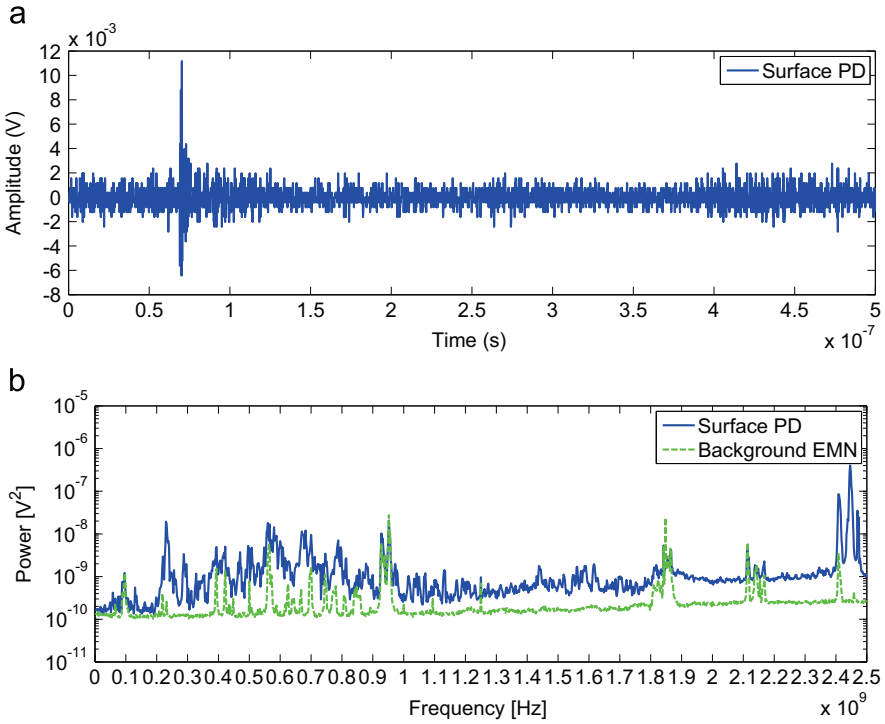

Fig. 13. RF pulse from the second PD source and its spectrum. (a) Surface PD pulse and (b) Surface PD spectrum.

Table 1
Summary of time–power ratios for the EM sources measured.

Source	PRL (%)	PRH (%)	t_{eff} average (ns)
Background EMN	10–31	18.7–62.8	32.6
Wi-Fi	1.5–6	2–20	58
Fluorescent ignition	40–98	2–50	14.8
Corona PD	22–70	14.6–57	7.3
Surface PD	6–25	9–41	2

that correspond to other events, quite possibly from PD activity. In the separation process, it is possible that several clusters are overlapped in the PR maps but including the pulse duration, the clouds appear separated in the time axis. Then, the pulses from the non-characterized clusters can be analysed in time and frequency to identify them.

Acknowledgements

Tests were done in the High-Voltage Research and Test Laboratory (LINEALT) at Universidad Carlos III de Madrid.

References

[1] Sharifi R, Ebrahimi M. Detection of stator winding faults in induction motors using three-phase current monitoring. ISA Trans 2011;50(1):14–20 ISSN 0019-0578, http://dx.doi.org/10.1016/j.isatra.2010.10.008.
[2] Gill P. Electrical power equipment maintenance and testing power engineering (Willis). 2nd ed., 2008 CRC Press, Taylor & Francis Group, Boca Raton FL, USA, ISBN 9781574446562.
[3] Boggs SA. Partial discharge. III. Cavity-induced PD in solid dielectrics. Electr Insul Mag IEEE 1990;6(November (6)):11–6. http://dx.doi.org/10.1109/57.63094 ISSN 0883-7554.
[4] Kreuger FH. Partial discharge detection in high-voltage equipment. 1989 Butterworth-Heinemann Ltd, Oxford, UK, ISBN 9780408020633.
[5] IEC-60270. High-voltage test techniques—partial discharge measurements, 3rd ed.; 2000.
[6] Judd MD, Farish O, Hampton BF. Broadband couplers for UHF detection of partial discharge in gas-insulated substations. Sci Meas Technol IEE Proc 1995;142(3):237–43. http://dx.doi.org/10.1049/ip-smt:19951699 ISSN 1350-2344.
[7] Shibuya Y, Matsumoto S, Tanaka M, Muto H, Kaneda Y. Electromagnetic waves from partial discharges and their detection using patch antenna. IEEE Trans Dielectr Electr Insul 2010;17(June (3)):862–71. http://dx.doi.org/10.1109/TDEI.2010.5492260 ISSN 1070-9878.
[8] Moore PJ, Portugues IE, Glover IA. Radiometric location of partial discharge sources on energized high-voltage plant. IEEE Trans Power Deliv 2005;20(July (3)):2264–72. http://dx.doi.org/10.1109/TPWRD.2004.843397 ISSN 0885-8977.
[9] Tenbohlen S, Denissov D, Hoek SM, Markalous SM. Partial discharge measurement in the ultra high frequency UHF range. IEEE Trans Dielectr Electr Insul 2008;15(December(6)):1544–52. http://dx.doi.org/10.1109/TDEI.2008.4712656 ISSN 1070-9878.
[10] Baker PC, Stephen B, Judd MD. Compositional modeling of partial discharge pulse spectral characteristics. IEEE Trans Instrum Meas 2013;62(July
[11] Gao Wensheng, Ding Dengwei, Liu Weidong, Huang Xinhong. Analysis of the intrinsic characteristics of the partial discharge induced by typical defects in GIS. IEEE Trans Dielectr Electr Insul 2013;20(June (3)):782–90. http://dx.doi.org/10.1109/TDEI.2013.6518948 ISSN 1070-9878.
[12] Peiqing Miao, Xiuwei Li, Yue Hu, Gehao Sheng, Xiuchen Jiang. Multi-source separation method for partial discharge detection in substations. In: Power engineering and automation conference (PEAM), 2012 IEEE; September 2012. p. 1–5.http://dx.doi.org/10.1109/PEAM.2012.6612543.
[13] Umamaheswari R, Sarathi R. Identification of partial discharges in gas-insulated switchgear by ultra-high-frequency technique and classification by adopting multi-class support vector machines. Electr Power Components Syst 2011;39(14):1577–95. http://dx.doi.org/10.1080/15325008.2011.596506.
[14] Ardila-Rey J, Martinez-Tarifa J, Robles G, Rojas-Moreno M. Partial discharge and noise separation by means of spectral-power clustering techniques. IEEE Trans Dielectr Electr Insul 2013;20(August (4)):1436–43. http://dx.doi.org/10.1109/TDEI.2013.6571466 ISSN 1070-9878.
[15] Gibson PJ. The Vivaldi aerial. In: Ninth European microwave conference, 1979; September 1979. p. 101–5. http://dx.doi.org/10.1109/EUMA.1979.332681.
[16] Janaswamy R, Schaubert DH. Dispersion characteristics for wide slotlines on low-permittivity substrates short paper. IEEE Trans Microw Theory Tech 1985;33(August (8)):723–6. http://dx.doi.org/10.1109/TMTT.1985.1133064 ISSN 0018-9480.
[17] Robles G, Albarracín R, Vázquez-Roy JL, Rajo-Iglesias E, Mártinez-Tarifa JM, Rojas-Moreno MV, et al. On the use of Vivaldi antennas in the detection of partial discharges. In: 2013 IEEE international conference on solid dielectrics (ICSD); June 2013. p. 302–5. http://dx.doi.org/10.1109/ICSD.2013.6619887.
[18] Balanis Constantine A. Antenna theory: analysis and design. 3rd ed., 2005 John Wiley & Sons, Inc., Hoboken, New Jersey, USA, Canada, ISBN 047166782X.
[19] Kreuger FH, Gulski E, Krivda A. Classification of partial discharges. IEEE Trans Electr Insul 1993;28(December (6)):917–31. http://dx.doi.org/10.1109/14.249365 ISSN 0018-9367.